UNIVERSITY OF CALIFORNIA SAN DIEGO

Allosteric regulation of RPTPα

A Thesis submitted in satisfaction of the requirements
for the degree Master of Science

in

Biology

by

Yutao Wen

Committee in charge:

Nunzio Bottini, Chair
Li-Fan Lu, Co-chair
Barry Grant

2019

The Thesis of Yutao Wen is approved, and it is acceptable in quality and form for publication on microfilm and electronically:

Co-Chair

Chair

University of California San Diego

2019

DEDICATION

In recognition of Dr. Nunzio Bottini for his source of knowledge, industry towards nurturing scientists, and enthusiasm for science.

TABLE OF CONTENTS

LIST OF ABBREVIATIONS

BSA	Bovine serum albumin
CST	Cell Signaling Technology
DMEM	Dulbecco's Modified Eagle Media
DMSO	Dimethyl sulfoxide
Bis-Tris	Bis-tris methane
DiFMU	6,8-Difluoro-7-Hydroxy-4-Methylcoumarin
DiFMUP	6,8-Difluoro-4-Methylumbelliferyl Phosphate
DMSO	Dimethyl sulfoxide
DTT	Dithiothreitol
D1	Domain 1
D2	Domain 2
EDTA	Ethylenediamine tetraacetic acid
FACS	Fluorescence-Activated Cell Sorting
FBS	Fetal bovine serum
IC	Intracellular
MES	2-(*N*-morpholino) ethanesulfonic acid
MU	7-Hydroxy-4-Methylcoumarin
MUP	4-Methylumbelliferyl Phosphate
*p*NPP	*p*-nitrophenyl phosphate
PTK	Protein Tyrosine Kinase
PTP domain	Phospho-Tyrosine Phosphatase domain
r.m.s.d.	root mean square deviation
RPTP	Receptor Protein Tyrosine Phosphatase
TLS	translation libration screw
Tris	tris (hydroxymethyl) aminomethane.

LIST OF FIGURES

LIST OF TABLES

LIST OF SUPPLEMENTAL FIGURES

ACKNOWLEDGEMENTS

I would like to acknowledge Professor Nunzio Bottini, my chair and thesis advisor of the program, for his support by providing with resources and guidance. His earnest and prudence towards science shall not be underappreciated. I would also like to acknowledge Dr. Eugenio Santelli who started this project for his hands-on supervision throughout the past two years. His patience and detailed advice are indispensable to the achievement of this project.

I would like to thank the staff at the Advanced Light Source at Lawrence Berkeley National Laboratory for assistance with remote X-ray data collection.

This thesis, in full, has been submitted for publication of the material and is coauthored with Shen Yang, Kuninobu Wakabayashi, Mattias N. D. Svensson, Stephanie M. Stanford, Eugenio Santelli, and Nunzio Bottini. The thesis author was the primary investigator and author of this material.

ABSTRACT OF THE THESIS

Allosteric regulation of RPTPα

by

Yutao Wen

Master of Science in Biology

University of California San Diego, 2019

Professor Nunzio Bottini, Chair
Professor Li-Fan Lu, Co-Chair

Protein Tyrosine Phosphatases (PTPs) are drug target candidates due to their role in signal transduction and involvement in various pathologies. Difficulty in developing orthosteric inhibitors of PTPs suitable for therapeutic purposes has raised interest in the development of allosteric inhibitors, yet no allosteric regulatory model has been formulated for most PTP subtypes. For the two PTPs, belonging to two distinct subtypes, for which such mechanisms have been characterized, SHP2 and PTP1B, they

have paved the way to development of specific inhibitors which show promise for future development of small molecule therapeutics. In this study we achieved the formulation and *in vitro* validation of a novel structure-based allosteric model for RPTPα and discuss its mechanistic implications, potential for drug discovery and possible applicability to other PTPs.

INTRODUCTION

Receptor-type Protein Tyrosine Phosphatase α (RPTPα) is an important positive regulator of SRC kinase activation and a known promoter of cancer growth, fibrosis and arthritis. The domain structure of RPTPs comprises an extracellular region, a transmembrane helix, and two tandem intracellular catalytic domains referred as D1 and D2. The D2 domain of RPTPs is believed to mostly play a regulatory function, however no regulatory model has been established for RPTPα-D2 or other RPTP-D2 domains. Here, we solved the crystal structure of the cytoplasmic region of RPTPα, encompassing D1 and D2, trapped in a conformation that highlights a possible mechanism through which D2 is able to allosterically inhibit D1 activity. By using an RPTPα D2-truncation mutant and mutational analysis of the D1/D2 interfaces, we showed that D2 inhibits RPTPα phosphatase activity and identified a $P^{405}FTP^{408}$ motif in D1 that mediates the inhibitory effect of D2. Expression of the gain of function F406A/T407A RPTPα mutant in HEK293T cells led to enhanced SRC activation, supporting the relevance of our proposed D2-mediated regulation mechanism in cell signaling. Given the emerging interest in the development of allosteric inhibitors of RPTPs, and the scarcity of validated allosteric sites for RPTPs, our study not only sheds light on the regulatory role of RPTP-D2 domains, but also provides a potentially useful tool for the discovery of chemical probes targeting RPTPα and other RPTPs.

Protein tyrosine phosphatases (PTPs) are a large subfamily of protein phosphatases that play essential roles in signal transduction by counteracting the action of protein tyrosine kinases (PTKs) and have been demonstrated to regulate a wide range of cellular processes, including cell proliferation, differentiation, migration, cell cycle, and metabolic homeostasis (1). Classical PTPs are characterized by a ~300 amino-acid conserved catalytic (PTP) domain (2,3) and categorized into receptor- and non-receptor- type PTPs (1,4). The human genome encodes 20 receptor PTPs (RPTPs), classified in 8 subtypes, which comprise an N-terminal extracellular domain of divergent function, sequence and structure, a transmembrane domain and one or two PTP domains (1,4). Receptor-type Protein Tyrosine

Phosphatase α (RPTPα) is encoded by the PTPRA gene and, together with Receptor-type Protein Tyrosine Phosphatase ε (RPTPε), defines the R4 RPTP subtype, characterized by a short, highly glycosylated extracellular domain of unknown function, a membrane-spanning domain, and two tandem cytoplasmic catalytic domains referred to as D1 (membrane-proximal) and D2 (membrane-distal). Despite the structural similarities between D1 and D2 domains, most or all of the catalytic activity in D1+D2 PTPs resides on D1, while D2 is believed to have regulatory and substrate recognition functions (5-13). However, the mechanism of such regulatory action of the RPTPs D2 domain has mostly remained undefined. RPTPα has been shown to be regulated by dimerization and the observation of an inaccessible active site in the dimeric crystal structure of its isolated D1 domain led to the proposed "wedge" model, in which an N-terminal helix-turn-helix "wedge" motif formed by the two N-terminal helices (α1', α2') of one monomer inhibits catalytic activity of the other monomer by insertion into its active site (14,15). It has been suggested that oxidation of the D2 domain of RPTPα regulates phosphatase activity by modifying the relative conformation of phosphatase dimers (7). However, the canonical D1-D2 arrangement seen in several subsequent RPTP structures encompassing both domains proved incompatible with the wedge model, thus it remains unclear whether the model applies to all RPTPs (2,3,16,17).

At the core of the active site of classical PTP domains there is a signature $HCX_5R(S/T)$ motif, included in the so called "P loop" containing a nucleophilic cysteine, and an arginine side chain responsible for coordinating the phosphate moiety and stabilizing the negative charge on the protein-substrate complex and the transition state (18). The same arginine is also responsible for triggering a switch from an inactive, open to an active, closed conformation of the other prominent structural element of the active site, the WPD loop, named after its conserved Trp-Pro-Asp motif, upon substrate binding (18,19). The catalytic reaction proceeds via two irreversible catalytic steps: the formation of a phospho-cysteine intermediate and its

breakdown and dissociation of the phosphate group. The aspartic acid in the WPD loop acts as a general acid to facilitate the nucleophilic attack in the first step by protonating the leaving group oxygen of the substrate and as a general base in the second step by deprotonating a water molecule that attacks the phospho-cysteine group to release a phosphate ion (18). Crucially, WPD loop closure has been shown to be rate-determining for the reaction catalyzed by both the model phosphatase PTP1B and the highly active *Yersinia* YopH, suggesting that PTP activity can be regulated by controlling WPD loop kinetics (20) and rationalizing the inhibitory effect of ligands that prevent WPD loop closure (21).

Activation of the SRC kinase by dephosphorylation of its C-terminal inhibitory Tyr^{530} in many cell types has emerged as a major mechanism through which RPTPα contributes to diverse processes such as cell proliferation and survival, cell cycle arrest, fibroblast migration, neuronal migration and differentiation, and integrin signaling (22-25). RPTPα is an established tumor promoter and a cancer target. Recent studies from the Downey laboratory and our laboratory also demonstrated RPTPα's ability to promote transforming growth factor β (TGFβ) signaling in lung fibroblasts and cell motility via the focal adhesion kinase (FAK) pathway in synovial fibroblasts. Loss of RPTPα protected mice from lung fibrosis and arthritis, suggesting additional indications for RPTPα inhibitors besides cancer (25,26).

Despite the fact that RPTPα and several other PTPs have been validated as potential drug targets, development of orthosteric small molecule inhibitors of PTPs has proven problematic due to both the charged nature and the high structural conservation of the active site (27,28). Recently, non-active site inhibitors have been identified for SHP2 and PTP1B, two medically relevant PTPs for which allosteric regulation mechanisms have been uncovered and

characterized (21,29-32). The promise of non-competitive inhibitors of PTPs has ignited interest in the discovery of novel allosteric mechanisms for the regulation of RPTP activity, however currently the allosteric regulation of RPTP-D1 domains remain mostly undefined. For PTP1B, evidence is mounting for the presence of an extended allosteric network centered on helix α7, whose position is determined by subtle conformational shifts in its surrounding structural elements (α3, α6, L11) and which in turn affects WPD loop closure (29-31) via a $P^{185}ESP^{188}$ motif ($P^{405}FTP^{408}$ in RPTPα and consensus sequence PXXP/A in D1+D2 RPTPs, where X=any amino-acid, see Supplemental Fig. S1) located at the C-terminal end of the WPD loop.

Here, to explore the possible allosteric regulation of RPTPα -D1, we report the first crystal structure of the cytoplasmic domain of RPTPα (D1D2). Through kinetic analysis and site-directed mutagenesis, we demonstrate that D2 is able to inhibit D1 catalytic activity. Our data suggest D2-mediated restriction of D1-WPD loop function, and we validate our resulting inhibition model in HEK293T cells. Our model helps unravel the physiological function of RPTP-D2 domains and could pave the way to future discovery of allosteric inhibitors for RPTPα and potentially other D1+D2 RPTPs.

MATERIALS & METHODS

Cloning, mutagenesis, protein expression and purification

For protein expression, a codon-optimized ORF encoding for a cytoplasmic fragment of human RPTPα (residues 202-793) encompassing the tandem catalytic domains (GenScript) was subcloned into the NcoI/XhoI site of pET28a (Novagen) and expressed in Escherichia coli BL21(DE3) as a C-terminal 6-Histidine fusion. Bacterial cultures were grown at 37 °C and induced with isopropyl 1-thio-β-d-galactopyranoside at room temperature for >12 hours. After recovery from the soluble fraction of the cell extract, RPTPα was purified by Ni-NTA affinity chromatography (Qiagen), anion exchange on a POROS 20 HQ column (ThermoFisher) and size exclusion chromatography (ENrich SEC 650, Bio-rad). Typical yields were 20 mg of purified protein per liter of culture. For RPTPε and RPTPσ, the corresponding DNA fragments (residues 104-699 and 1331-1916, respectively) were amplified from a mouse full-length cDNA and cloned into the NcoI/XhoI site of pET28a and the NdeI/XhoI site of pET26b (Novagen), respectively. All mutants were generated by standard site-directed mutagenesis techniques and purified following the same procedures. For eukaryotic expression, a plasmid encoding full length mouse RPTPα with an HA epitope tag at C-terminus in pCDNA3.1(+) at restriction sites AflII and XhoI was purchased from GenScript. Mutants were generated by standard site-directed mutagenesis techniques. All mutations were confirmed by DNA sequencing. All primers used were synthesized by Integrated DNA Technologies.

Crystallization and X-ray crystallography

Crystals of RPTPα 202-793 grew in 3-7 days by sitting or hanging drop vapor diffusion against a buffer containing 6% PEG 20000, 100 mM 2-(*N*-morpholino) ethanesulfonic acid (MES), pH 6, 10 mM DTT at a protein concentration of 6 mg/ml. Crystals belonged to Space Group $P2_12_12$ with Unit Cell parameters a=112.1 Å, b=136.4 Å, c=104.7 Å and two molecules per Asymmetric Unit. A complete native dataset to 1.8 Å resolution was collected at 100 K using 25% glycerol as cryoprotectant from a

single crystal at beamline 5.0.1 of the Advanced Light Source and processed using imosflm (44). The structure was solved by molecular replacement in PHASER (45) using the structure of mouse RPTPα 202-503 (PDB code 1YFO (14)) for both tandem domains, followed by initial automatic model rebuilding/refinement with buccaneer (46) and manual model building in coot (47) and refinement with refmac5 (48). TLS refinement was used with one TLS group per PTP domain. Data quality was analyzed with Rampage (49). Data collection and refinement statistics are summarized in Table 1. Molecular graphics objects were generated with Chimera (50).

Phosphatase activity assays

For assays using DiFMUP as a substrate, the protein was diluted to 2 nM in buffer 2xT1 (100 mM Tris pH 7.3, 20 mM DTT, 0.02% Triton X-100), and various concentrations (800 μM, 400 μM, 200 μM, 80 μM, 40 μM, 20 μM, 8 μM, 0 μM) of DiFMUP (Invitrogen) were prepared in 8% DMSO. 25 μL of protein solution and 25 μL of DiFMUP solution were mixed on a 96-well solid black polystyrene microplate (Corning) and DiFMU formation was continuously monitored by measuring its fluorescence at wavelengths of 358 (excitation) and 455 (emission) nm on a Tecan Infinite M1000 plate reader for 20 minutes. To convert fluorescence readings into DiFMU formation rates, a series of calibration curves were generated by combining known amounts of DiFMU and DiFMUP in assay buffer to yield total concentrations equal to each initial DiFMUP concentration in the assay. A calibration factor was calculated for each DiFMU + DiFMUP concentration as the slope of the fluorescence vs. DiFMU concentration. Initial reaction rates were fitted to a Michaelis-Menten equation of V= Kcat [Enzyme] [S] / (Km + [S]) by GraphPad Prism 8. For assays using MUP as a substrate, the protein was diluted to 25 nM in buffer 2xT2 (100 mM Bis-Tris 6.0, 20 mM DTT, 0.02% Triton X-100), and various concentrations (16 mM, 8 mM, 4 mM, 1.6 mM, 0.8 mM, 0.4 mM, 0.16 mM, 0 mM) of MUP (free acid, Biotium) buffered at pH 6.0 were prepared in 8% DMSO. 12.5 μL of protein solution and 12.5 μL of MUP solution were mixed on a Corning 96 Well solid black polystyrene microplate at 0, 2, 4, 6, 8, 10

minutes and all reactions were stopped by adding 25 μL of 1 M NaOH followed by fluorescence measurement with wavelengths of 358 (excitation) and 455 (emission) nm on a Tecan Infinite M1000 plate reader. Fluorescence readings were converted into 7-Hydroxy-4-methyl coumarin (Acros, abbreviated here as MU) formation rates using a similar procedure as described above for DiFMUP/DiFMU. Initial reaction rates were fitted to a Michaelis-Menten equation of V= Kcat [Enzyme] [S] / (Km + [S]) by GraphPad Prism 8.

Transient transfection of HEK293T cells

HEK293T cells were cultured in Corning Dulbecco's modified Eagle's medium (with 4.5 g/L glucose, L-glutamine, sodium pyruvate) with 10% fetal bovine serum (BioFluid Technologies) at 37 °C and 5% CO2. Transient transfections were carried out in standard 6-well cell culture plates (Corning) with 2.5 μg plasmid using three different transfection reagents, linear polyethylenimine (Sigma), FuGENE (Promega) or Lipofectamine 3000 (ThermoFisher), in Opti-MEM medium (Gibco). The medium was changed to 10% FBS-containing medium after 12 hours and the cells were harvested after 24 hours.

Flow cytometry

Transfected HEK293T cells were trypsinized and resuspended in FACS buffer (2.5% FBS, 1 mM EDTA, 0.01% NaN_3). Cells were stained with Fixable Viability dye eFluor™ 780 (eBioscience/Thermo Fisher) to select live cells. Cells were then fixed in IC fixation buffer (Invitrogen) and FACS buffer 1:1 at room temperature for 30 minutes and permeabilized in ice-cold methanol on ice for 30 minutes. Permeabilized cells were then incubated with Fc block (BD Pharmingen) and stained with anti-HA antibodies conjugated with Alexa Fluor 488 (CST) for 1 hour, followed with another staining with Mouse anti-SRC (pY419; clone K98-37) antibodies conjugated with Alexa Fluor 647 (BD Biosciences) for 1 hour. Cells were analyzed on a Bio-Rad ZE5 Cell Analyzer, and collected data was analyzed using FlowJo software (Tree Star, Inc.).

Statistical Analysis

The statistical analyses utilized for each experiment are reported in the figure legends. Non-parametric stats were used unless data were assessed as fitting a normal distribution by Shapiro-Wilk test. Significance of one-way ANOVA tests was corrected for multiple comparisons using the Tukey test.

RESULTS

Crystal structure of the tandem catalytic domains of RPTPα

We crystallized a large C-terminal cytoplasmic region of RPTPα, comprising D1 and D2 (residues 202-793, hereafter referred to as $RPTP\alpha^{WT}$) and solved its crystal structure by molecular replacement to a resolution of 1.8 Å (Table 1). The protein crystallizes as a monomer, consistent with

Table 1. Crystallographic data collection and refinement statistics.

Data Collection	**Overall (last shell)**
Resolution (Å)	30-1.8 (1.83-1.80)
Wavelength (Å)	0.97741
Space Group	$P2_12_12$
Unit Cell	
a, b, c (Å)	112.1, 136.4, 104.7
α, β, γ (°)	90, 90, 90
Unique Reflections	148737 (7290)
Completeness	100 (100)
Multiplicity	6.2 (5.7)
I/σ(I)	10.6 (1.9)
R_{pim}	0.037 (0.401)
$CC_{1/2}$	0.998 (0.751)
Wilson B Factor (Å^2)	23.0
Refinement	**Overall (last shell)**
Resolution (Å)	30-1.80 (1.85-1.80)
Reflections Used	141157 (10297)
R_{work} / R_{free}	0.155/0.191 (0.261/0.286)
Non-H protein Atoms	9682
Solvent Atoms	1529
Average B Factor (Å^2)	38.2
Protein Main/Side Chain A	30.8/39.2
Protein Main/Side Chain B	34.8/43.0
Solvent	45.9
r.m.s.d. Bond Lengths (Å)	0.006
r.m.s.d. Bond Angles (°)	1.48
Ramachandran Plot	
Favored (%)	97.0
Allowed (%)	2.8
Disallowed (%)	0.2

previous reports (3) as well as size exclusion data from the present work (not shown), with two molecules per asymmetric unit (chains A, B). The final model contains residues 206-793 (chain A) and 207-789 with gaps at 226-227 and 515-520 (chain B) with 1529 solvent molecules and 57% solvent content and is in good agreement with the published structures of the isolated D1 and D2 domains of RPTPα (PDB codes 1YFO and 1Y15 (14,33)) with maximum root mean square deviation (r.m.s.d., all atoms) of 0.74 and 0.86 Å for D1 and D2, respectively. Ambiguous electron density was seen for residues 221-234 in molecule B, indicating the presence of more than one main chain path. The WPD loop in all subunits is in the open conformation, consistent with the absence of any active site ligands. The nomenclature and location of RPTPα secondary structure elements in relation to primary and tertiary structure are shown in Supplemental Fig. S1.

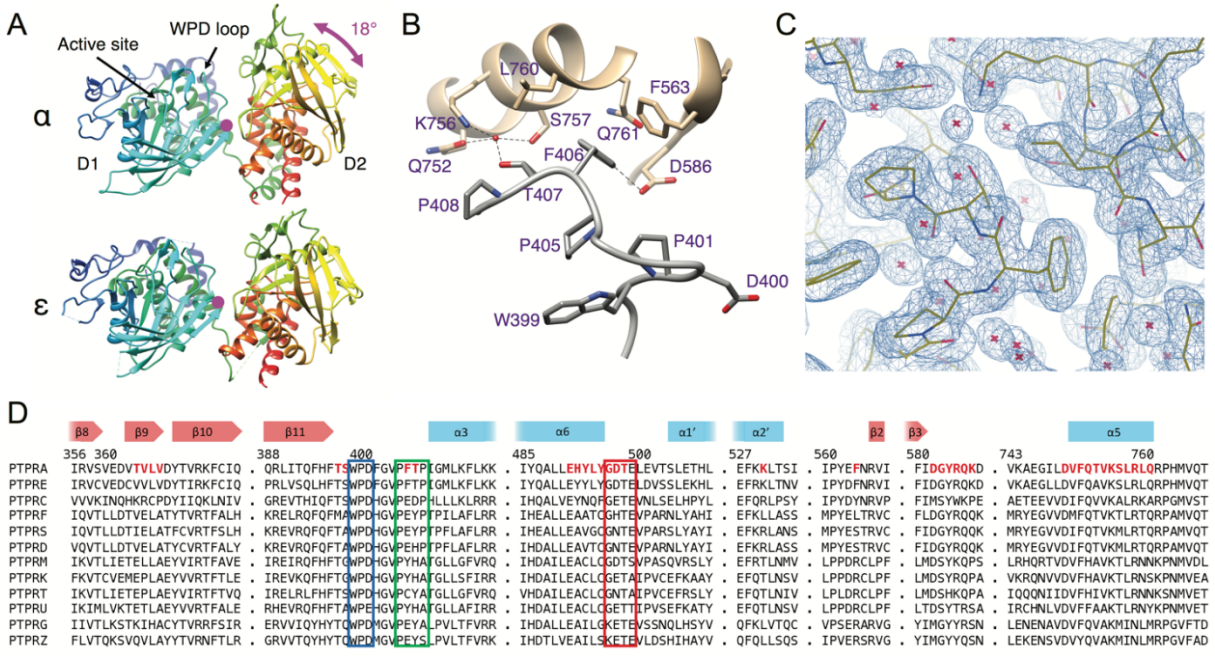

Figure 1. Comparison of the crystal structures of the tandem catalytic domains of RPTPε and RPTPα suggests interdomain flexibility and reveals an intramolecular contact between D2 and the PFTP motif in D1. (A) Ribbon representation of RPTPε and RPTPα showing an 18° rotation of D2 around an axis perpendicular to the plane of the figure (magenta dot) upon superposition of D1. The rotation brings D2 at interacting distance to the PFTP motif C-terminal to the WPD loop in D1.(B) Interdomain interaction between the PFTP in D1 (grey) and several residues in D2 (tan). Key interacting residues and structural elements are highlighted. (C) 2Fo-Fc electron density map around the same site as in Fig. 1B, contoured at 1.5σ. (D) Protein sequence alignment of the 12 D1+D2 human RPTPs around the sites of interdomain interaction. Stretches of RPTPα residues directly involved in the interaction are in red. The boxes highlight the alignment of the WPD (blue) and the PXXP/A motif (green) and the linker sequence. RPTPα secondary structure elements are shown at the top for reference.

An extensive network of interdomain interactions (summarized in Supplemental Fig. S2) provides stability to the typical architecture seen in other currently available tandem domain RPTP structures (2,3,16,17) (Fig. 1A). The previously described interactions between residues in strands β9 and β10 and helix α3 of D1 and the D2 β2-β3 loop helix α5 in D2 are also seen in our structure, albeit with differences due to the moderate sequence conservation across PTP subfamilies (Supplemental Fig. S1). The linker, of sequence $G^{496}DTE^{499}$, is constrained to adopt the same conformation as in LAR, RPTPσ, RPTPγ and CD45: a network of direct or water-mediated H-bonds connects the main-chain O of G496, the Oγ of T498, the side chains of E491 on D1 α6 and those of D750 and Q753 on D2 α5,

while D497 and E499 form salt bridges with K416 in D1 α3 and R742 in D2 α4 (see Supplemental Fig. S2). The D2 loop between β2 and β3 contributes a backbone H-bond between Y588 and V367 in the β9-β10 turn, while Nζ of K591 contacts Oγ of T397 and the main chain O of T367 (molecule A) and Nη of R589 contacts the main chain O of V365 (molecule B). The interface is further stabilized by shape and charge complementarity, as evidenced by several van der Waals and electrostatic interactions. In addition, the PXXP motif ($P^{405}FTP^{408}$ in RPTPα) in D1 interacts tightly with D2 residues in α4 and the region between α1 and β3, as shown in Fig. 1B. F406 closely contacts the side chains of Q761 through the face of its phenylalanine ring and D586 in an anion-π pair through its edge, at C-C distances of 3.3 and 3.6 Å, respectively, while the side chains of F563, L760 and S757 approach at van der Waals distances of 3.8. 4.0 and 4.1 Å. T407 contributes a water-mediated interaction with the side chains of Q753, K756 and S757. Fig. 1C shows the same region of the molecule in its 2Fo-Fc map contoured at 1.5 σ.

When we compared our structure with that of its closest homolog, RPTPε (PDB code 2JJD, chains A-F(3)) using DynDom (34), we noticed a 14 to 19 degree rotation of D2 with respect to D1 around an axis running roughly along the main interdomain interaction interface from the linker region to the β9-β10 turn. This rotation brings the WPD loop and helix α3 of RPTPα in closer contact with D2 (Fig. 1A). For comparison, rotation angles of 2 to 9 degrees, often with major components perpendicular to the same axis, were calculated between pairs of chains in 2JJD. Because residues at the D1/D2 interface and linker region are highly conserved between RPTPα and RPTPε (Fig. 1D), we speculated that the observed differences might reflect a degree of interdomain flexibility constrained as distinct rigid conformations by the crystal packing.

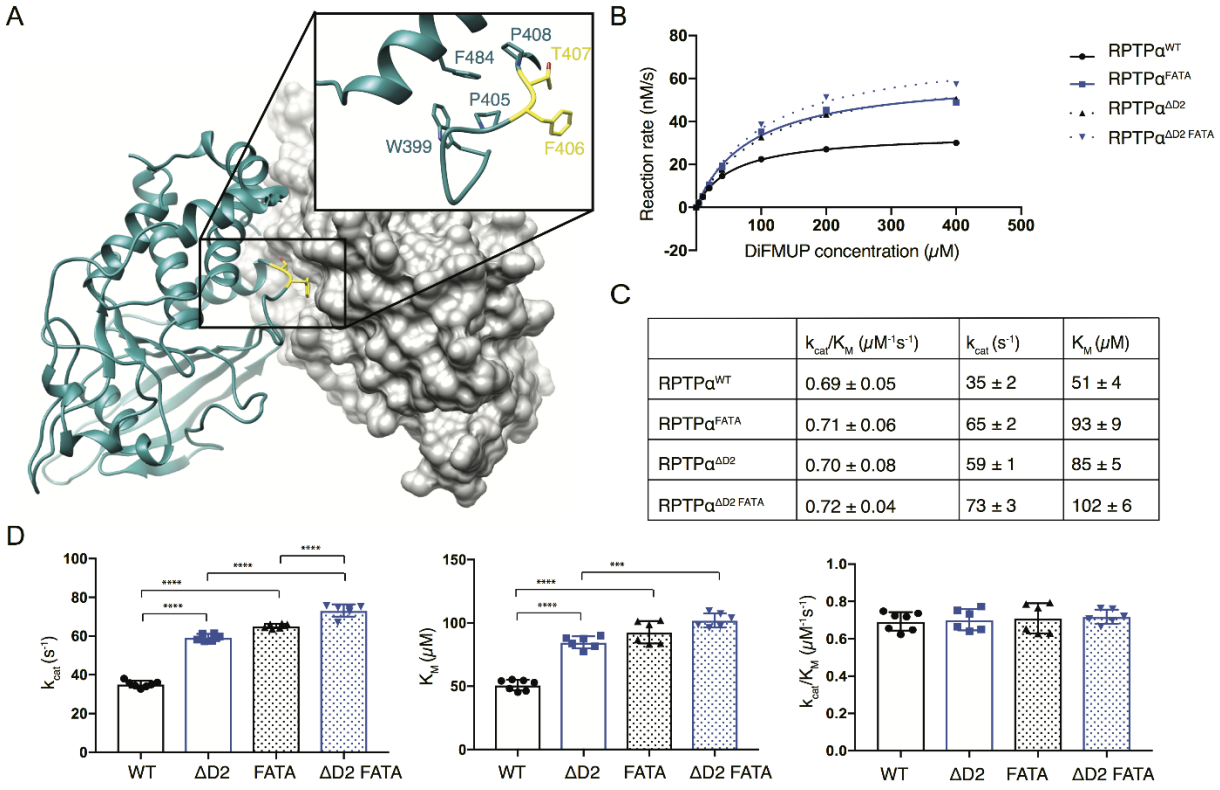

	k_{cat}/K_M ($\mu M^{-1}s^{-1}$)	k_{cat} (s^{-1})	K_M (μM)
RPTPα^{WT}	0.69 ± 0.05	35 ± 2	51 ± 4
RPTPα^{FATA}	0.71 ± 0.06	65 ± 2	93 ± 9
RPTPα$^{\Delta D2}$	0.70 ± 0.08	59 ± 1	85 ± 5
RPTPα$^{\Delta D2\ FATA}$	0.72 ± 0.04	73 ± 3	102 ± 6

Figure 2. RPTPα D2 domain regulates the catalytic activity of the D1 domain through the PFTP motif. (A) Ribbon representation of RPTPα D1 (blue) and solvent accessible surface representation of D2 (gray) with a detail of the PFTP motif (FT in yellow). (B) Representative Michaelis-Menten curves showing enzyme activity of RPTPα^{WT} and its mutants: RPTPα$^{\Delta D2}$, RPTPα^{FATA}, and RPTPα$^{\Delta D2\ FATA}$. Data points are presented as mean ± standard deviation. (C) Table summarizing k_{cat}, K_M, and k_{cat}/K_M of RPTPα^{WT} and mutants shown above. Data were calculated by averaging six individual experiments, each including three technical replicates (n=3) and are reported as average ± standard deviation. (D) Bar graph showing comparison of k_{cat}, K_M, and k_{cat}/K_M of RPTPα^{WT} and mutants above. Each data point represents one individual experiment with three technical replicates (n=3) and error bar represents the standard deviation. One-way ANOVA test was used (**** = $p<0.0001$, *** = $p<0.001$).

D2 regulates the catalytic activity of RPTPα

It has been observed that nearly all of RPTPα phosphatase activity resides at the D1 active site with little contribution from the D2 active site (9,35). We confirmed this observation in the context of our tandem D1D2 construct by mutating the active cysteine to serine in D1 (Cys433Ser, RPTPα^{D1CS}) or D2 (Cys723Ser, RPTPα^{D2CS}) and showing that D2 has negligible phosphatase activity on 6,8-Difluoro-4-Methylumbelliferyl Phosphate (DiFMUP) as substrate (data not shown). Despite D2's modest direct contribution to the enzymatic activity, the observation that, in the crystal structure of RPTPα, residues

in D2 come in close contact and restrict the conformational freedom of the crucial PXXP motif suggests that D2 might be able to directly regulate the activity of D1. Based on our structural information, the WPD loop freedom appears to be limited when the tandem domains are in the closed state, thus we formulated a model in which RPTPα activity is turned on and off by switching respectively between open and closed interdomain conformations. To test our model, we first compared the phosphatase activities of RPTPα^{WT} and the RPTPα$^{\Delta D2}$ mutant (residues 202-503) using DiFMUP as substrate (Fig. 2). RPTPα$^{\Delta D2}$ exhibited a turnover number (kcat) ~ 1.7 times that of RPTPα^{WT}. Increased substrate conversion rate in the absence of D2 is consistent with its potential involvement in an inhibitory mechanism that regulates RPTPαWT phosphatase activity. The effect of the ΔD2 and other RPTPα mutations on kcat/KM will be discussed in a dedicated section.

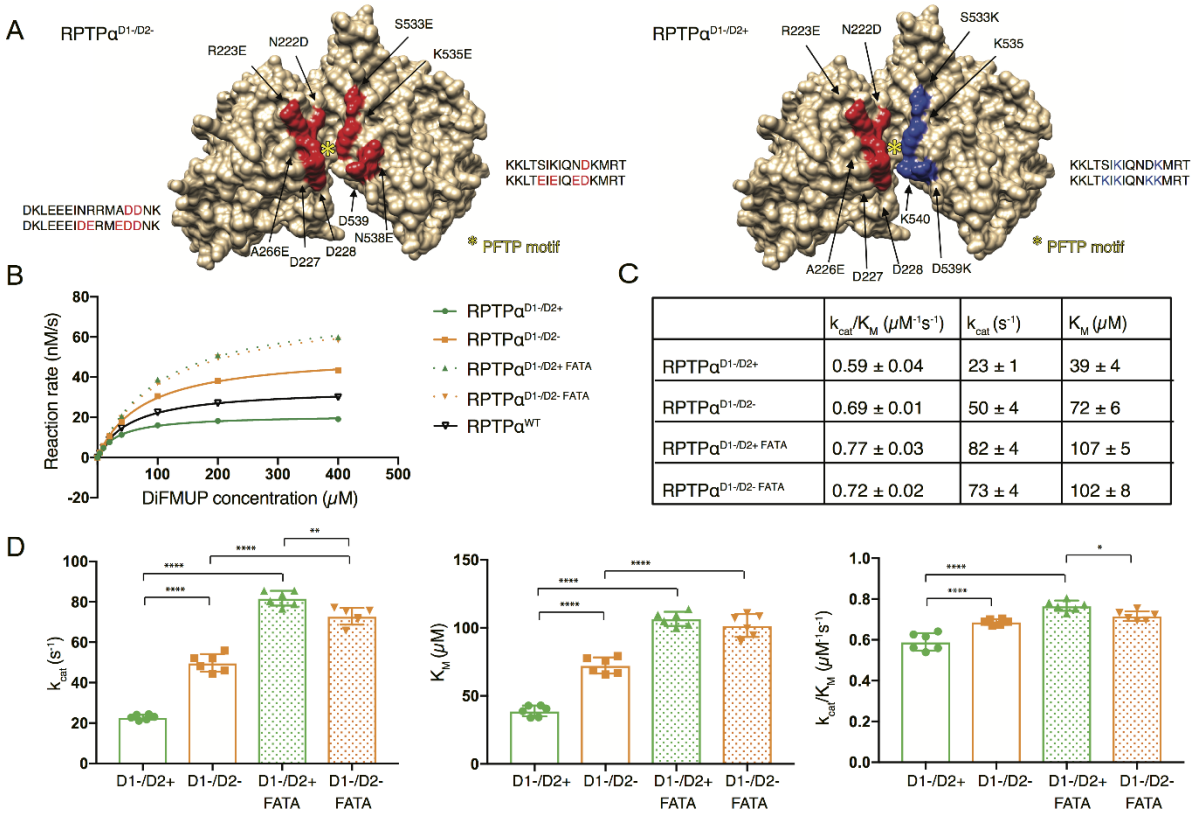

	k_{cat}/K_M ($\mu M^{-1}s^{-1}$)	k_{cat} (s^{-1})	K_M (μM)
RPTPα$^{D1-/D2+}$	0.59 ± 0.04	23 ± 1	39 ± 4
RPTPα$^{D1-/D2-}$	0.69 ± 0.01	50 ± 4	72 ± 6
RPTPα$^{D1-/D2+ FATA}$	0.77 ± 0.03	82 ± 4	107 ± 5
RPTPα$^{D1-/D2- FATA}$	0.72 ± 0.02	73 ± 4	102 ± 8

Figure 3. Altering the D1/D2 interface by charge-modifying mutagenesis affects catalytic activity. (A) Charge-modifying mutations were introduced facing the crevice between the two domains. Two mutants, RPTPα$^{D1-/D2+}$ and RPTPα$^{D1-/D2-}$, were generated and are shown mapped on the RPTPα structure as a solvent accessible surface representation. Red and blue residues indicate the presence of negatively and positively charged amino acids respectively. (B) Representative Michaelis-Menten curves showing enzymatic activity of the mutants: RPTPα$^{D1-/D2+}$, RPTPα$^{D1-/D2-}$, RPTPα$^{D1-/D2+ FATA}$, and RPTPα$^{D1-/D2- FATA}$. Data points are presented as mean ± standard deviation. (C) Table summarizing k_{cat}, K_M, and k_{cat}/K_M of the same mutants as in B. Data were calculated by averaging six individual experiments, each of which includes three technical replicates (n=3) and are reported as average ± standard deviation. (D) Bar graphs showing k_{cat}, K_M, and k_{cat}/K_M for each of the mutants above. Each data point represents one individual experiment with three technical replicates (n=3) and error bar represents standard deviation. One-way ANOVA test was used (**** = p<0.0001, ** = p<0.01, * = p<0.05).

Mutational analysis of the regulation of D1 activity by D2

We next sought to investigate the specific roles of residues in RPTPα P^{405}FTP^{408} motif (here called PFTP), corresponding to P^{185}ESP^{188} in PTP1B and PXXP/A in other RPTPs (Fig. 1D), in the D2-mediated RPTPα inhibition mechanism. We generated the RPTPα^{FATA} and RPTPα$^{\Delta D2 FATA}$ mutants by

substituting Ala for Phe^{406} and Thr^{407} in $RPTP\alpha^{WT}$ and $RPTP\alpha^{\Delta D2}$ respectively, in order to assess the effect of the intermolecular interaction between the PFTP motif and the D2 interface. As observed following the deletion of D2, the reaction rate of $RPTP\alpha^{FATA}$ was elevated (~1.8 times) compared to $RPTP\alpha^{WT}$ and similar (~1.1 times increase) to that of $RPTP\alpha^{\Delta D2}$, while $RPTP\alpha^{\Delta D2\ FATA}$ only showed a modest (~1.2 times) increase in kinetic activity compared to $RPTP\alpha^{\Delta D2}$. These data suggest that the PFTP motif exerts a D2-dependent inhibitory influence upon RPTPα-D1, although a small intrinsic activating effect of the FATA mutation on D1 activity is also measurable. These results point to a critical role of the D1-PFTP motif in the mechanism of phosphatase activity inhibition by D2.

For D2 to be able to inhibit the phosphatase activity of D1 in response to a change of their relative orientation in solution, $RPTP\alpha^{WT}$ must exist as an equilibrium between at least two (closed/open) and possibly a continuum of intermediate states. To further validate our model, we therefore introduced attractive or repulsive charges into D1 and D2, generating mutants $RPTP\alpha^{D1-/D2+}$ and $RPTP\alpha^{D1-/D2-}$ in order to shift the equilibrium towards a more closed or open structure. We chose residues in α1' of D1 and residues following α2' in D2 as the gap between these surfaces widens by 3-4 Å in the open state seen in RPTPε versus the closed state in RPTPα, while they are still sufficiently removed from the active site and the WPD loop to minimize any direct influence on the catalytic rates: for the D1- mutation the sequence E^{220}INRRMAD^{227} was replaced with EIDERMED, for the D2- and D2+ mutations L^{531}TSIKIQNDK^{540} was replaced respectively with LTEIEIQEDK and LTKIKIQNKK, as shown in Fig. 3A. As expected, the catalytic activity of $RPTP\alpha^{D1-/D2+}$ was significantly reduced compared to that of $RPTP\alpha^{D1-/D2-}$ (Fig. 3B). The turnover number of $RPTP\alpha^{D1-/D2-}$ was more than double that of $RPTP\alpha^{D1-/D2+}$. However, the difference was lost after the introduction of the FATA mutation ($RPTP\alpha^{D1-/D2-\ FATA}$ displayed a ~1.1 times decrease in turnover number compared to $RPTP\alpha^{D1-/D2+\ FATA}$). This observation is consistent with the effect of introducing attractive and repulsive charges in the D1/D2 interface being mediated by the PFTP motif and lends further support to a regulation mechanism by interdomain flexibility in RPTPα.

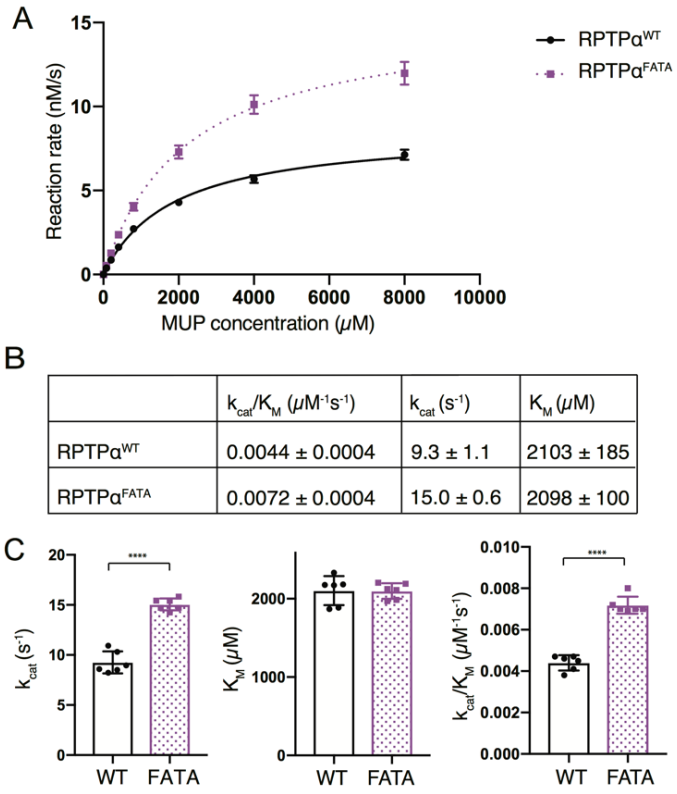

	k_{cat}/K_M ($\mu M^{-1}s^{-1}$)	k_{cat} (s^{-1})	K_M (μM)
RPTPα^{WT}	0.0044 ± 0.0004	9.3 ± 1.1	2103 ± 185
RPTPα^{FATA}	0.0072 ± 0.0004	15.0 ± 0.6	2098 ± 100

Figure 4. The PFTP motif limits D1 phosphatase activity by restricting WPD loop catalysis as suggested by its effect on kcat/KM using MUP as substrate. (A) Representative Michaelis-Menten curves showing enzyme activity of RPTPα^{WT} and RPTPα^{FATA} using MUP as substrate. Data points are presented as mean ± standard deviation. (B) Table summarizing k_{cat}, K_M, and k_{cat}/K_M of RPTPα^{WT} and RPTPα^{FATA} with MUP as substrate. Data were calculated by averaging six individual experiments and are reported as average ± standard deviation. (C) Bar graph showing comparison of k_{cat}, K_M, and k_{cat}/K_M of RPTPα^{WT} and RPTPα^{FATA}. Each data point represents one individual experiment and error bars represents standard deviation. T-test was used to compare two data sets (**** = $p<0.0001$).

Kinetic data support inhibition of D1-WPD loop catalysis by D2

To seek evidence in support of the involvement of the WPD loop in the allosteric regulation mediated by the PFTP motif, we took advantage of differences in the catalytic reaction mechanism between two PTP substrates, DiFMUP and the closely related 4-Methylumbelliferyl Phosphate (MUP, ThermoFisher Scientific). PTP catalysis proceeds via reversible substrate binding (step 1 in eq. A, where

ES represents the substrate-bound enzyme and EP the phospho-cysteine intermediate), followed by two irreversible steps, the formation (step 2) and breakdown (step 3) of a phospho-cysteine intermediate:

$$\mathrm{E + S} \underset{k_{-1}}{\overset{(1)\ k_1}{\rightleftharpoons}} \mathrm{ES} \overset{(2)\ k_2}{\rightarrow} \mathrm{EP} \overset{(3)\ k_3}{\rightarrow} \mathrm{E + P} \qquad \text{(A)}$$

In step 2, the aspartic acid in the WPD loop acts as a general acid by protonating the leaving group. In the phospho-cysteine breakdown (step 3), the aspartate acts as a base to facilitate the nucleophilic attack of a water molecule that dephosphorylates the cysteine. However, because the product of DiFMUP dephosphorylation (DiFMU) has a pKa of 4.7, due to the presence of two F substituents on the aromatic ring (36), dissociation of DiFMU is predicted not to require acid catalysis at the chosen physiological pH of 7.3. Therefore, as a consequence of the dissociative nature of the transition state (discussed in ref. (18)) the reaction rate of step 2 with DiFMUP as substrate will be relatively independent of WPD loop involvement. According to the Michaelis-Menten model for a two-step reaction under the quasi-steady state approximation, k_{cat}/K_M is solely dependent on the kinetics of substrate binding and the first irreversible catalytic step (18):

$$\text{(B)} \qquad K_M = \frac{k_3}{k_2+k_3}\,\frac{k_2+k_{-1}}{k_1}$$

$$\text{(C)} \qquad k_{cat} = \frac{k_2 k_3}{k_2+k_3}$$

$$\text{(D)} \qquad \frac{k_{cat}}{K_M} = \frac{k_2 k_1}{k_2+k_{-1}}$$

Thus, the observation that k_{cat} but not k_{cat}/K_M is strongly affected by mutations that abolish or relax the conformational restraints on the PFTP motif by D2 is consistent with the involvement of the WPD loop in the allosteric regulation that we propose in our model. When we assessed RPTPα^{FATA}-mediated dephosphorylation of MUP whose dephosphorylation product has a pKa of 7.8 (36), as a substrate at pH

6.0 (Fig. 4), we observed a significant increase of k_{cat}/K_M for RPTPα^{FATA} versus RPTPα^{WT}. This observation is consistent with the assumptions in our structure-based hypothesis described above.

Figure 5. The activity-modulating effect of D2 is present in RPTPσ but not RPTPε. (A) Sequence conservation between RPTPα and RPTPε mapped on the RPTPα solvent accessible surface. Identical residues are in yellow, non-identical residues in dark cyan. (B) Top: representative Michaelis-Menten curves showing enzyme activity of $RPTP\varepsilon^{WT}$ and mutants $RPTP\varepsilon^{FATA}$, $RPTP\varepsilon^{D1-/D2}$ and $RPTP\varepsilon^{D1-/D2+}$ using DiFMUP as substrate. Data points are presented as mean ± standard deviation. Bottom: table summarizing k_{cat}, K_M, and k_{cat}/K_M from the same experiment set. Data were calculated by averaging six individual experiments. All kinetic data are reported as average ± standard deviation. (C) The sequence conservation between RPTPα and RPTPσ mapped on the RPTPα solvent accessible surface as in A illustrates the relatively low identity between the two species. (D) Top: representative Michaelis-Menten curves showing enzyme activity of $RPTP\sigma^{WT}$ and mutants $RPTP\sigma^{FATA}$ using DiFMUP as substrate. Data points are presented as mean ± standard deviation. Bottom: table summarizing k_{cat}, K_M, and k_{cat}/K_M for the same experiment set. Data were calculated by averaging six individual experiments. T-test was used to compare two data sets (**** = $p<0.0001$, *** = $p<0.001$). (E) Top: representative Michaelis-Menten curves showing enzyme activity of $RPTP\sigma^{WT}$ and mutants $RPTP\sigma^{FATA}$ using MUP as substrate. Data points are presented as mean ± standard deviation. Bottom: table summarizing k_{cat}, K_M, and k_{cat}/K_M for the same experiment set. Data were calculated by averaging six individual experiments. T-test was used to compare two data sets (**** = $p<0.0001$, *** = $p<0.001$).

A

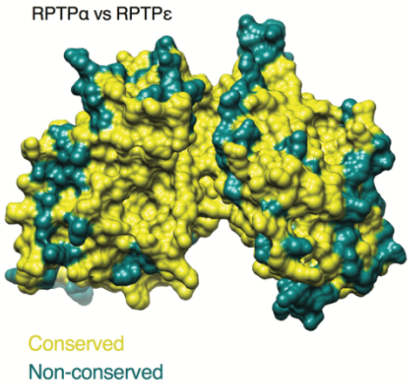

B

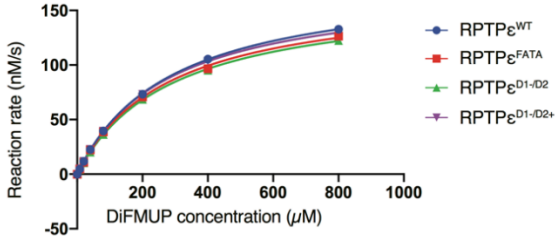

	k_{cat}/K_M ($\mu M^{-1} s^{-1}$)	k_{cat} (s^{-1})	K_M (μM)
RPTPε^{WT}	0.65 ± 0.03	184 ± 7	281 ± 10
RPTPε^{FATA}	0.64 ± 0.03	166 ± 9	260 ± 20
RPTPε$^{D1-/D2}$	0.58 ± 0.01	159 ± 12	275 ± 19
RPTPε$^{D1-/D2+}$	0.65 ± 0.01	172 ± 8	265 ± 13

C

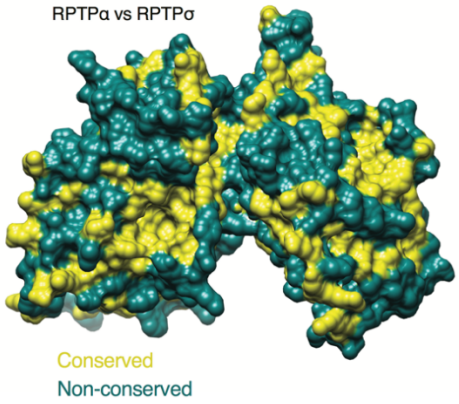

D

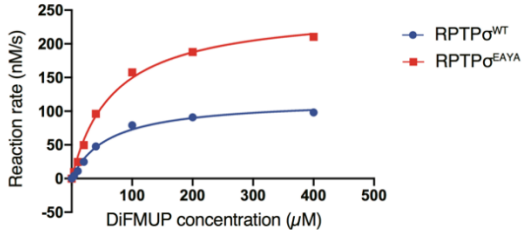

	k_{cat}/K_M ($\mu M^{-1} s^{-1}$)****	k_{cat} (s^{-1})****	K_M (μM)***
RPTPσ^{WT}	2.20 ± 0.15	134 ± 14	68 ± 16
RPTPσ^{EAYA}	3.59 ± 0.16	332 ± 24	107 ± 12

E

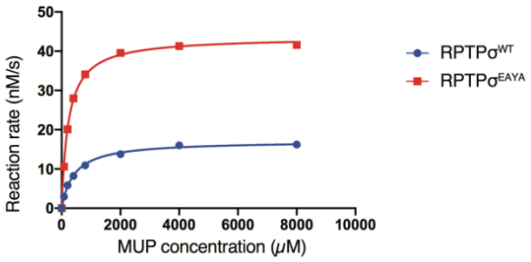

	k_{cat}/K_M ($\mu M^{-1} s^{-1}$)****	k_{cat} (s^{-1})****	K_M (μM)***
RPTPσ^{WT}	0.051 ± 0.006	17.9 ± 2.0	357 ± 58
RPTPσ^{EAYA}	0.213 ± 0.014	40.4 ± 4.7	190 ± 31

Conservation of the PXXP-mediated inhibitory mechanism in other RPTPs

To examine whether our hypothesized RPTPα inhibitory mechanism is conserved in RPTPε, we introduced mutations homologous to those described above for RPTPα into RPTPε, thus generating the RPTPε^{FATA} (Phe307Ala, Thr308Ala), RPTPε$^{D1-/D2}$ and RPTPε$^{D1-/D2+}$. Here we replaced the sequence E^{122}IRVRSAD^{129} with EIDERSED for the D1- mutation and the sequence L^{432}TNVRIMKENM^{442} with LTKVRIMKKKM for the D2+ mutation. Somewhat surprisingly, given the 70% sequence identity and surface homology between RPTPε and RPTPα within the catalytic domains (Fig. 5A), all the above mentioned RPTPε mutants displayed similar kinetics when using DiFMUP as substrate (Fig. 5B), indicating that the regulatory mechanism via the PFTP motif described for RPTPα is not echoed in RPTPε, at least under the experimental conditions employed. This observation is however consistent with the more open interdomain configuration, and the consequent increased distance between the PXXP motif and D2, in all six independent molecules in the crystal structure of RPTPε (3). On the contrary, when we considered the more distantly related RPTPσ (Fig. 1D and 5C), mutation of RPTPσ P^{1520}EYP^{1523} to PAAP (referred to as RPTPσ^{EAYA}) led to a greater than two-fold increase in phosphatase activity compared to RPTPσ^{WT} (Fig. 5D and E). This phenomenon was observed using both DiFMUP and MUP as substrates, mirroring what was seen with the corresponding RPTPα mutants, albeit with differences, namely a marked decrease and a smaller than expected increase in K_M when using MUP and DiFMUP, respectively. While these differences in catalytic parameters are possibly due to electrostatic effects following the loss of a negative charge, the observed behavior of RPTPσ mutants is in agreement with the close approach between D2 and the PXXP motif in the three available crystal structures of the tandem catalytic domain of RPTPσ (PDB codes 2FH7, 3SR9, 4BPC (3,37,38)). Although more subtle than in our RPTPα structure, a similar interaction in RPTPσ occurs between the aromatic ring of Y1522 and the side chains of E1521 in D1, with the side chains of T1876, and S1678 in D2, respectively (3).

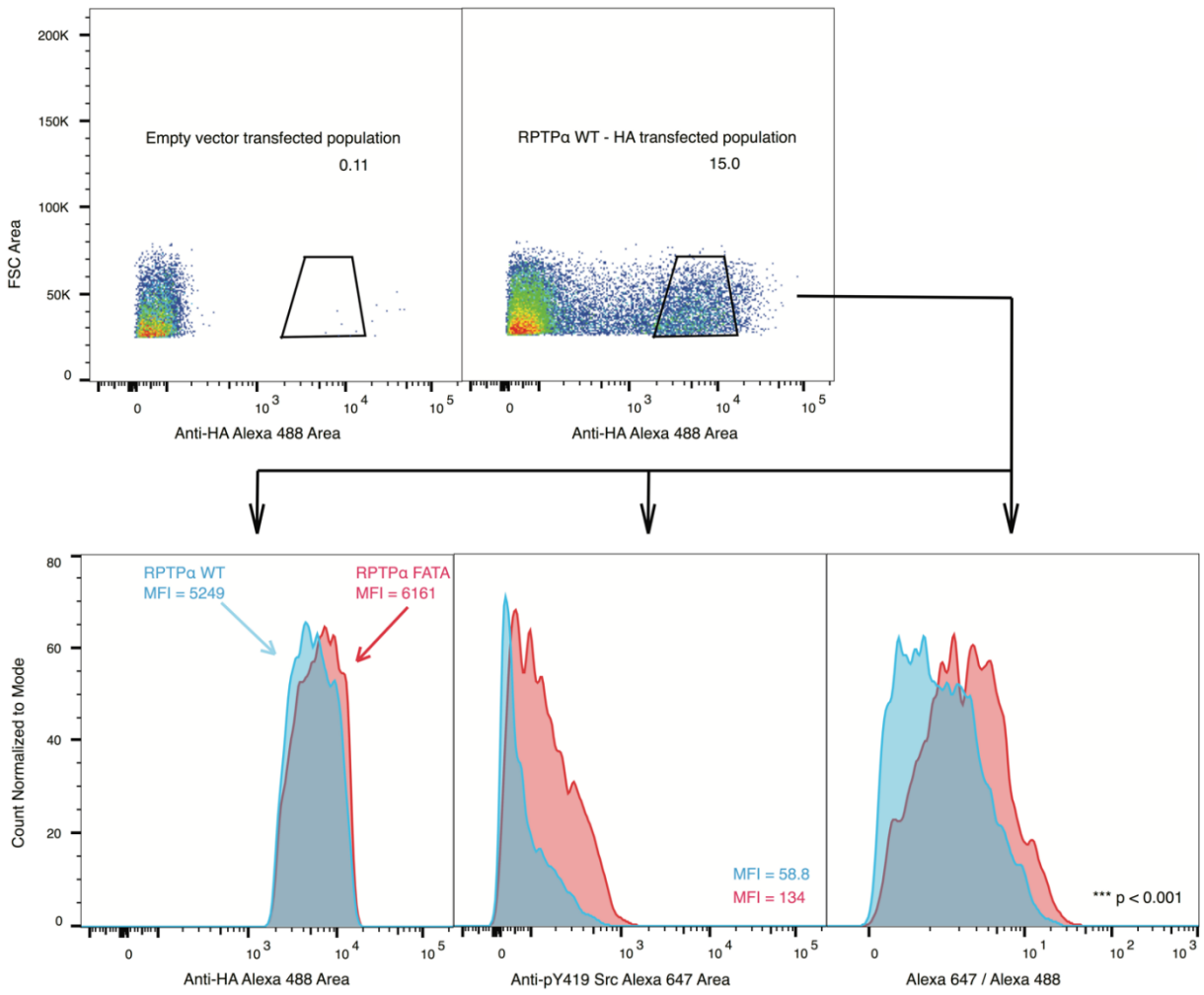

Figure 6. HEK293T cells overexpressing RPTPα^{FATA} display higher phosphorylation of SRC Y419 than HEK293T cells with similar overexpression of RPTPα^{WT}. RPTPα ^{WT} and RPTPα ^{FATA} HA-tagged transfected HEK293T cells were stained with anti-HA Alexa488-conjugated antibody and anti-pY419 SRC Alexa647-conjugated antibody and analyzed by flow cytometry. Live single cells with high RPTPα ^{WT} and RPTPα ^{FATA} expression were gated (upper panels), and Alexa488 (anti-HA), Alexa647 (anti-phosphoSRC [Y419]), and the ratio of Alexa647/Alexa488 were assessed and plotted on histograms (lower panels). Panels are representative of 4 independent experiments with similar results. Kolmogorov-Smirnov test was used to compare two data sets (*** = p<0.001).

Overexpression of RPTPα^{FATA} promotes SRC activation in HEK293T cells

Because RPTPα is known to dephosphorylate the SRC kinase on its inhibitory Y^{530}, leading to increased activity and phosphorylation at the activating Y^{419} (39,40), we sought to indirectly measure RPTPα phosphatase activity in cells by detecting phospho-SRC (Y419) levels in cells overexpressing

RPTPα. We therefore overexpressed HA-tagged RPTPα^{WT} or RPTPα^{FATA} in HEK293T cells and analyzed phosphorylation of SRC by phospho-flow cytometry in populations of cells gated for expression of HA-RPTPα. Consistent with our *in-vitro* observation of an elevated phosphatase activity of RPTPα^{FATA}, the median fluorescence intensity of phospho-SRC (Y^{419}) was tripled in cells expressing RPTPα^{FATA} compared with cells expressing similar levels of RPTPα^{WT} (Fig. 6). These data suggest that RPTPα^{FATA} phosphatase activity towards its natural substrate SRC is increased with respect to RPTPα^{WT} in HEK293T cells, thus validating our model of allosteric regulation of RPTPα in a cellular context.

DISCUSSION

The allosteric regulation of PTP activity has gained attention in recent years in light of the increasing number of validated drug targets among PTPs (41) and the therapeutic promise offered by the discovery of non-competitive modulators of PTP1B (14,21,29,31) and SHP2 (32). It was suggested that D2 of RPTPs could regulate the activity of D1 in a manner similar to the role of helix α7 in PTP1B based on molecular architecture conservation (31). Our result showing that the presence of D2 roughly halves the activity of D1 *in vitro* is consistent with a previous study in which *p*-nitrophenyl phosphate (*p*NPP) was used as substrate (9), but such mechanism has not been demonstrated yet in detail. In this work, we describe the characterization, at the structural level, of a mechanism of D2-mediated regulation of D1 for RPTPα, a positive regulator of SRC which is considered a drug target for cancer, fibrosis and rheumatoid arthritis. Our study is one of the first examples of structure-based assessment of the potential regulatory role of an RPTP-D2 on D1 activity. A recent report has described non-competitive inhibition of RPTPσ by DJ001 and related compounds, which are believed to bind to the D1/D2 interface of RPTPσ (42) - an enzyme that shares with RPTPα the PXXP-mediated D2 regulatory mechanism. However, the mechanism of action of DJ001 has not yet been investigated via structural biology and/or mutagenesis.

The regulatory mechanism described in our study could be relevant to the discovery of inhibitors of RPTPα and likely other RPTPs, if compounds that are able to stabilize the closed interdomain conformation of the RPTPs can be identified. Although a small inhibitory effect of D2 persists in our RPTPα^{FATA} mutant - possibly due to residual D1-D2 interaction - (Fig. 2), we speculate that RPTPα^{FATA} could become a useful tool for counterscreening RPTPα inhibitors and selectively identifying those that act through the above-mentioned mechanism. However, a caveat of targeting the D1/D2 interface for drug discovery purposes is its relatively high level of conservation between different RPTPs. With regard to this point, the apparent lack of conservation of the D2-mediated regulation mechanism between RPTPα and RPTPε in *in vitro* assays is intriguing and unexpected based on the high conservation

between these two members of the R4 subtype. Further investigations are warranted to understand the biochemical mechanisms underlying such divergent behavior, for example by assessing the relative weight of local non-conserved residues vs global molecular dynamic differences.

A limitation of our study is the fact that, while the geometry we observe in our crystal structure is fully closed with respect to the D1/D2 interface, we have no information about the equilibrium that likely exists in solution between open and closed populations. We were unable to reliably measure RPTPα catalytic activity in the crystal itself, or to generate mutants that would lock the closed state in solution by Cys-Cys cross-linking (data not shown). As a result, we could not achieve any assessment of whether any residual activity is present in the closed form of the enzyme. These considerations are relevant to the exploitation of the D1/D2 interface for discovery of non-competitive inhibitors since the activity of the closed form would likely reflect the highest *in vitro* inhibition achievable. Similarly, we originally modeled the mechanism of allosteric D2-mediated regulation of RPTPα D1 based on the observation of a downward movement of the $P^{185}XXP^{188}$ motif of PTP1B in concert with WPD loop closure (20) and the conservation of the crucial PTP1B residue P^{185} involved in the so called CH/π switch to stabilize the closed WPD loop conformation (30). However, no structure of RPTPα with a closed WPD loop is available at this time and the role of the CH/π switch has not been formally demonstrated for PTPs other than PTP1B. Therefore, as the D2 can affect catalytic activity by destabilizing the closed WPD conformation or by slowing down its dynamics, we cannot distinguish between these two possibilities on the basis of our kinetic analysis alone.

Mutagenesis of the PXXP motif of recombinant RPTPα-D1D2 and of RPTPα overexpressed in HEK293T cells led to a similar gain of function behavior. These data strongly suggest that our model of D2-mediated regulation of D1 activity via the PXXP motif is valid for full length RPTPα expressed in a cellular context. However, despite evidence of its significance in cells, we cannot speculate further about the physiological relevance of the allosteric mechanism in question. There is no known post-

translational regulation of the D1/D2 interface of RPTPα and RPTPε and/or ligands of their ectodomains. Thus, we currently have a limited ability to investigate whether the mechanism might be subjected to physiological regulation and/or contributes to the modulation of RPTPα activity in response to cell stimuli. Interestingly, some of the weakest and/or ambiguous electron densities, suggestive of a possible protein-protein interaction area, are found at amino-acids 221-334, around the α1'-a2' turn in D1, and 534-542, C-terminal to α2' in D2, roughly coincident with the blue and red colored regions in Fig. 3. We speculate that simultaneous binding of a ligand to both patches or its interaction with the 40-residue linker connecting D1 to the transmembrane helix could tether together or force apart D1 and D2 and modulate catalytic activity. Given the role D2 can play in substrate recognition (10,12,13), an intriguing possibility is that D2 regulates phosphatase activity by simultaneous substrate binding and enzyme activation.

An area worthy of future investigation is the potential relationship between the allosteric mechanism described here and the dimerization of RPTPα. Two mechanisms have been proposed to mediate outside-in signaling of RPTPs involving dimerization of their intracellular domains, namely the aforementioned "wedge" hypothesis and a head-to-toe dimer in which D2 blocks access to the D1 active site via a pair of Asp residues at its β10-β11 turn. The latter was initially suggested on the basis of the crystal structure of RPTPγ (3) and subsequently confirmed *in vitro* and *in vivo* for RPTPζ (43), but since the same dimeric arrangement is not present in other crystal structures of RPTPs and the Asp-Asp sequence is not generally conserved at the same position, this feature is likely to be limited to the R5 subtype. As mentioned, the "wedge" dimer is mutually exclusive with the typical organization of D1+D2 RPTP. A structural superposition of RPTPα D1D2 onto the D1 dimer (PDB code 1YFO (14)) reveals that only one copy of D2 needs to be displaced from its position in order to accommodate the second subunit in the dimer. Such assembly can be predicted to have increased inter-monomer buried surface due to novel D1-D2 intermolecular contacts and could either occur in cells under appropriate circumstances, such as oxidation of D2 Cys723 by reactive oxygen species and consequent partial

unfolding of the N-terminal region of D2 (7), or represent a mechanism of cross-regulation between different RPTPs.

In conclusion, we have described here a novel mechanism of regulation of RPTPα activity by the D1/D2 interface via a conserved PXXP motif in the D1 domain. Despite the above-mentioned limitations, we believe our study is a significant initial step toward unraveling the allosteric regulation of RPTPs. The latter is one of the least understood areas of PTP biology, but potentially relevant to enable the drugging of these enzymes for the treatment of multiple human diseases.

This thesis, in full, has been submitted for publication of the material and is coauthored with Shen Yang, Kuninobu Wakabayashi, Mattias N. D. Svensson, Stephanie M. Stanford, Eugenio Santelli, and Nunzio Bottini. The thesis author was the primary investigator and author of this material.

REFERENCES

1. Tonks, N. (2006) Protein tyrosine phosphatases: from genes, to function, to disease. *Nature Reviews Molecular Cell Biology* **7**, 833-846

2. Almo, S. C., Bonanno, J. B., Sauder, J. M., Emtage, S., Dilorenzo, T. P., Malashkevich, V., Wasserman, S. R., Swaminathan, S., Eswaramoorthy, S., Agarwal, R., Kumaran, D., Madegowda, M., Ragumani, S., Patskovsky, Y., Alvarado, J., Ramagopal, U. A., Faber-Barata, J., Chance, M. R., Sali, A., Fiser, A., Zhang, Z.-Y., Lawrence, D. S., and Burley, S. K. (2007) Structural genomics of protein phosphatases. *Structural genomics of protein phosphatases* **8**, 121-140

3. Barr, A., Ugochukwu, E., Lee, W., King, O., Filippakopoulos, P., Alfano, I., Savitsky, P., Burgess-Brown, N., Muller, S., and Knapp, S. (2009) Large-Scale Structural Analysis of the Classical Human Protein Tyrosine Phosphatome. *Cell* **136**, 352-363

4. Alonso, A., Sasin, J., Bottini, N., Friedberg, I., Osterman, A., Godzik, A., Hunter, T., Dixon, J., and Mustelin, T. (2004) Protein tyrosine phosphatases in the human genome. *Cell* **117**, 699-711

5. Streuli, M., Krueger, N. X., Thai, T., Tang, M., and Saito, H. (1990) Distinct functional roles of the two intracellular phosphatase like domains of the receptor-linked protein tyrosine phosphatases LCA and LAR. *EMBO J* **9**, 2399-2407

6. Wallace, M., Fladd, C., Batt, J., and Rotin, D. (1998) The second catalytic domain of protein tyrosine phosphatase delta (PTP delta) binds to and inhibits the first catalytic domain of PTP sigma. *Molecular and Cellular Biology* **18**, 2608-2616

7. Blanchetot, C., Tertoolen, L., and den Hertog, J. (2002) Regulation of receptor protein-tyrosine phosphatase alpha by oxidative stress. *Embo Journal* **21**, 493-503

8. Toledano-Katchalski, H., Tiran, Z., Sines, T., Shani, G., Granot-Attas, S., den Hertog, J., and Elson, A. (2003) Dimerization in vivo and inhibition of the nonreceptor form of protein tyrosine phosphatase epsilon. *Molecular and Cellular Biology* **23**, 5460-5471

9. Lim, K., Lai, D., Kalousek, M., Wang, Y., and Pallen, C. (1997) Kinetic analysis of two closely related receptor-like protein-tyrosine-phosphatases, PTP alpha and PTP epsilon. *European Journal of Biochemistry* **245**, 693-700

10. Kashio, N., Matsumoto, W., Parker, S., and Rothstein, D. M. (1998) The second domain of the CD45 protein tyrosine phosphatase is critical for interleukin-2 secretion and substrate recruitment of TCR-zeta in vivo. *J Biol Chem* **273**, 33856-33863

11. Wang, Y., Guo, W., Liang, L., and Esselman, W. (1999) Phosphorylation of CD45 by casein kinase 2 - Modulation of activity and mutational analysis. *Journal of Biological Chemistry* **274**, 7454-7461

12. Felberg, J., Lefebvre, D., Lam, M., Wang, Y., Ng, D., Birkenhead, D., Cross, J., and Johnson, P. (2004) Subdomain X of the kinase domain of Lck binds CD45 and facilitates dephosphorylation. *Journal of Biological Chemistry* **279**, 3455-3462

13. Tsujikawa, K., Kawakami, N., Uchino, Y., Ichijo, T., Furukawa, T., Saito, H., and Yamamoto, H. (2001) Distinct functions of the two protein tyrosine phosphatase domains of LAR (leukocyte common antigen-related) on tyrosine dephosphorylation of insulin receptor. *Molecular Endocrinology* **15**, 271-280

14. Bilwes, A., denHertog, J., Hunter, T., and Noel, J. (1996) Structural basis for inhibition of receptor protein-tyrosine phosphatase-alpha by dimerization. *Nature* **382**, 555-559

15. Jiang, G., den Hertog, J., Su, J., Noel, J., Sap, J., and Hunter, T. (1999) Dimerization inhibits the activity of receptor-like protein-tyrosine phosphatase-alpha. *Nature* **401**, 606-610

16. Nam, H., Poy, F., Krueger, N., Saito, H., and Frederick, C. (1999) Crystal structure of the tandem phosphatase domains of RPTP LAR. *Cell* **97**, 449-457

17. Nam, H., Poy, F., Saito, H., and Frederick, C. (2005) Structural basis for the function and regulation of the receptor protein tyrosine phosphatase CD45. *Journal of Experimental Medicine* **201**, 441-452

18. Zhang, Z. (2003) Mechanistic studies on protein tyrosine phosphatases. *Progress in Nucleic Acid Research and Molecular Biology, Vol 73* **73**, 171-220

19. Pannifer, A. D., Flint, A. J., Tonks, N. K., and Barford, D. (1998) Visualization of the cysteinyl-phosphate intermediate of a protein-tyrosine phosphatase by x-ray crystallography. *J Biol Chem* **273**, 10454-10462

20. Whittier, S., Hengge, A., and Loria, J. (2013) Conformational Motions Regulate Phosphoryl Transfer in Related Protein Tyrosine Phosphatases. *Science* **341**, 899-903

21. Wiesmann, C., Barr, K., Kung, J., Zhu, J., Erlanson, D., Shen, W., Fahr, B., Zhong, M., Taylor, L., Randal, M., McDowell, R., and Hansen, S. (2004) Allosteric inhibition of protein tyrosine phosphatase 1B. *Nature Structural & Molecular Biology* **11**, 730-737

22. Gu, Z., Fang, X., Li, C., Chen, C., Liang, G., Zheng, X., and Fan, Q. (2017) Increased PTPRA expression leads to poor prognosis through c-Src activation and G1 phase progression in squamous cell lung cancer. *International Journal of Oncology* **51**, 489-497

23. Hao, Q., Rutherford, S., Low, B., and Tang, H. (2006) Selective regulation of hydrogen peroxide signaling by receptor tyrosine phosphatase-alpha. *Free Radical Biology and Medicine* **41**, 302-310

24. Zeng, L., D'Alessandri, L., Kalousek, M., Vaughan, L., and Pallen, C. (1999) Protein tyrosine phosphatase alpha (PTP alpha) and contactin form a novel neuronal receptor complex linked to the intracellular tyrosine kinase fyn. *Journal of Cell Biology* **147**, 707-713

25. Stanford, S., Svensson, M., Sacchetti, C., Pilo, C., Wu, D., Kiosses, W., Hellvard, A., Bergum, B., Muench, G., Elly, C., Liu, Y., den Hertog, J., Elson, A., Sap, J., Mydel, P., Boyle, D., Corr, M., Firestein, G., and Bottini, N. (2016) Receptor Protein Tyrosine Phosphatase alpha-Mediated Enhancement of Rheumatoid Synovial Fibroblast Signaling and Promotion of Arthritis in Mice. *Arthritis & Rheumatology* **68**, 359-369

26. Aschner, Y., Khalifah, A., Briones, N., Yamashita, C., Dolgonos, L., Young, S., Campbell, M., Riches, D., Redente, E., Janssen, W., Henson, P., Sap, J., Vacaresse, N., Kapus, A., McCulloch, C., Zemans, R., and Downey, G. (2014) Protein Tyrosine Phosphatase alpha Mediates Profibrotic Signaling in Lung Fibroblasts through TGF-beta Responsiveness. *American Journal of Pathology* **184**, 1489-1502

27. Stanford, S. M., and Bottini, N. (2017) Targeting Tyrosine Phosphatases: Time to End the Stigma. *Trends Pharmacol Sci* **38**, 524-540

28. Zhang, Z. Y. (2017) Drugging the Undruggable: Therapeutic Potential of Targeting Protein Tyrosine Phosphatases. *Acc Chem Res* **50**, 122-129

29. Cui, D., Beaumont, V., Ginther, P., Lipchock, J., and Loria, J. (2017) Leveraging Reciprocity to Identify and Characterize Unknown Allosteric Sites in Protein Tyrosine Phosphatases. *Journal of Molecular Biology* **429**, 2360-2372

30. Choy, M., Li, Y., Machado, L., Kunze, M., Connors, C., Wei, X., Lindorff-Larsen, K., Page, R., and Peti, W. (2017) Conformational Rigidity and Protein Dynamics at Distinct Timescales Regulate PTP1B Activity and Allostery. *Molecular Cell* **65**, 644-+

31. Keedy, D., Hill, Z., Biel, J., Kang, E., Rettenmaier, T., Brandao-Neto, J., Pearce, N., von Delft, F., Wells, J., and Fraser, J. (2018) An expanded allosteric network in PTP1B by multitemperature crystallography, fragment screening, and covalent tethering. *Elife* **7**

32. Chen, Y., LaMarche, M., Chan, H., Fekkes, P., Garcia-Fortanet, J., Acker, M., Antonakos, B., Chen, C., Chen, Z., Cooke, V., Dobson, J., Deng, Z., Fei, F., Firestone, B., Fodor, M., Fridrich, C., Gao, H., Grunenfelder, D., Hao, H., Jacob, J., Ho, S., Hsiao, K., Kang, Z., Karki, R., Kato, M., Larrow, J., La Bonte, L., Lenoir, F., Liu, G., Liu, S., Majumdar, D., Meyer, M., Palermo, M., Perez, L., Pu, M., Price, E., Quinn, C., Shakya, S., Shultz, M., Slisz, J., Venkatesan, K., Wang, P., Warmuth, M., Williams, S., Yang, G., Yuan, J., Zhang, J., Zhu, P., Ramsey, T., Keen, N., Sellers, W., Stams, T., and Fortin, P. (2016) Allosteric inhibition of SHP2 phosphatase inhibits cancers driven by receptor tyrosine kinases. *Nature* **535**, 148-+

33. Sonnenburg, E., Bilwes, A., Hunter, T., and Noel, J. (2003) The structure of the membrane distal phosphatase domain of RPTP alpha reveals interdomain flexibility and an SH2 domain interaction region. *Biochemistry* **42**, 7904-7914

34. Hayward, S., and Berendsen, H. (1998) Systematic analysis of domain motions in proteins from conformational change: New results on citrate synthase and T4 lysozyme. *Proteins-Structure Function and Genetics* **30**, 144-154

35. Wu, L., Buist, A., denHertog, J., and Zhang, Z. (1997) Comparative kinetic analysis and substrate specificity of the tandem catalytic domains of the receptor-like protein-tyrosine phosphatase alpha. *Journal of Biological Chemistry* **272**, 6994-7002

36. Sun, W., Gee, K., and Haugland, R. (1998) Synthesis of novel fluorinated coumarins: Excellent UV-light excitable fluorescent dyes. *Bioorganic & Medicinal Chemistry Letters* **8**, 3107-3110

37. Hou, L., Wang, J., Zhou, Y., Li, J., and Zang, Y. (2011) Structural insights into the homology and differences between mouse protein tyrosine phosphatase-sigma and human protein tyrosine phosphatase-sigma. *Acta Biochim Biophys Sin (Shanghai)* **43**, 977-988

38. Jeon, T. J., Chien, P. N., Chun, H. J., and Ryu, S. E. (2013) Structure of the catalytic domain of protein tyrosine phosphatase sigma in the sulfenic acid form. *Mol Cells* **36**, 55-61

39. Zheng, X. M., Wang, Y., and Pallen, C. J. (1992) Cell transformation and activation of pp60c-src by overexpression of a protein tyrosine phosphatase. *Nature* **359**, 336-339

40. Su, J., Muranjan, M., and Sap, J. (1999) Receptor protein tyrosine phosphatase alpha activates Src-family kinases and controls integrin-mediated responses in fibroblasts. *Curr Biol* **9**, 505-511

41. He, R., Yu, Z., Zhang, R., and Zhang, Z. (2014) Protein tyrosine phosphatases as potential therapeutic targets. *Acta Pharmacologica Sinica* **35**, 1227-1246

42. Zhang, Y., Roos, M., Himburg, H., Termini, C., Quarmyne, M., Li, M., Zhao, L., Kan, J., Fang, T., Yan, X., Pohl, K., Diers, E., Gim, H., Damoiseaux, R., Whitelegge, J., McBride, W., Jung, M., and Chute, J. (2019) PTP sigma inhibitors promote hematopoietic stem cell regeneration. *Nature Communications* **10**

43. Fujikawa, A., Sugawara, H., Tanga, N., Ishii, K., Kuboyama, K., Uchiyama, S., Suzuki, R., and Noda, M. (2019) A head-to-toe dimerization has physiological relevance for ligand-induced inactivation of protein tyrosine receptor type Z. *J Biol Chem* **294**, 14953-14965

44. Battye, T., Kontogiannis, L., Johnson, O., Powell, H., and Leslie, A. (2011) iMOSFLM: a new graphical interface for diffraction-image processing with MOSFLM. *Acta Crystallographica Section D-Biological Crystallography* **67**, 271-281

45. Mccoy, A., Grosse-Kunstleve, R., Adams, P., Winn, M., Storoni, L., and Read, R. (2007) Phaser crystallographic software. *Journal of Applied Crystallography* **40**, 658-674

46. Cowtan, K. (2006) The Buccaneer software for automated model building. 1. Tracing protein chains. *Acta Crystallographica Section D-Biological Crystallography* **62**, 1002-1011

47. Emsley, P., Lohkamp, B., Scott, W., and Cowtan, K. (2010) Features and development of Coot. *Acta Crystallographica Section D-Biological Crystallography* **66**, 486-501

48. Murshudov, G., Vagin, A., and Dodson, E. (1997) Refinement of macromolecular structures by the maximum-likelihood method. *Acta Crystallographica Section D-Structural Biology* **53**, 240-255

49. Lovell, S., Davis, I., Adrendall, W., de Bakker, P., Word, J., Prisant, M., Richardson, J., and Richardson, D. (2003) Structure validation by C alpha geometry: phi,psi and C beta deviation. *Proteins-Structure Function and Genetics* **50**, 437-450

50. Pettersen, E. F., Goddard, T. D., Huang, C. C., Couch, G. S., Greenblatt, D. M., Meng, E. C., and Ferrin, T. E. (2004) UCSF Chimera--a visualization system for exploratory research and analysis. *J Comput Chem* **25**, 1605-1612